

Computational Strategies in Discovering Novel Non-nucleoside Inhibitors of HIV-1 RT

Maria Letizia Barreca,^{*,‡} Angela Rao,^{*,‡} Laura De Luca,[‡] Maria Zappalà,[‡] Anna-Maria Monforte,[‡] Giovanni Maga,[‡] Christophe Pannecouque,[§] Jan Balzarini,[§] Erik De Clercq,[§] Alba Chimirri,[‡] and Pietro Monforte[‡]

Dipartimento Farmaco-Chimico, Università di Messina, Viale Annunziata, 98168 Messina, Italy, Istituto di Genetica Molecolare IGM-CNR, via Abbiategrasso 207, 27100 Pavia, Italy, and Rega Institute for Medical Research, Katholieke Universiteit Leuven, Minderbroedersstraat 10, B-3000 Leuven, Belgium

Received September 2, 2004

A three-dimensional common feature pharmacophore model was developed using the X-ray structure of RT/non-nucleoside inhibitor (NNRTI) complexes. Starting from the pharmacophore hypothesis and the structure of the lead compound TBZ, new NNRTIs were designed and synthesized, having the benzimidazol-2-one system as a scaffold. Docking experiments showed that these molecules docked in a position and orientation similar to that of known inhibitors. Biological testing confirmed that our strategy was successful in searching for new leads as NNRTIs.

Introduction

NNRTIs are an important class of anti-AIDS drugs increasingly used in combination therapy together with the previously approved nucleoside/nucleotide RTIs and protease inhibitors.¹ NNRTIs are a structurally diverse group of compounds interacting with a specific allosteric nonsubstrate binding site of HIV-1 RT, thus leading to a noncompetitive inhibition of the enzyme. They cause a conformational change that disrupts the catalytic site and blocks DNA polymerase activity.² After having focused our researches on the identification of new molecules with anti-RT activity,^{3,4} we have now used different computational methods in attempts to gather additional information for our rational design and to discover new classes of NNRTIs.

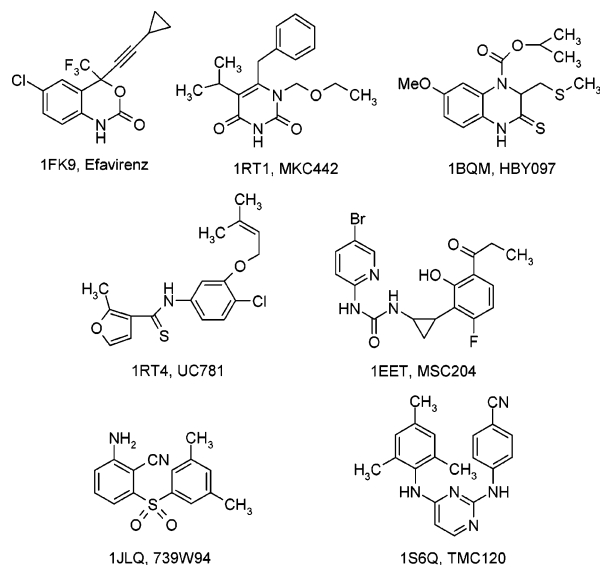
We started on the X-ray crystal structures of different ligand/enzyme complexes, showing both the bioactive conformations of the inhibitors and their interactions with the residues of the RT binding pocket. Such structural data together with molecular modeling enhance the process of drug design. A hypothetical 3-D pharmacophore model for NNRTIs was built by using a combined ligand- and structure-based molecular modeling approach. The postulated hypothesis allowed us to design and synthesize a new potential class of NNRTIs, and the antiviral activity results confirmed the strength of our rational approach.

Results and Discussion

Pharmacophore Modeling. Several cocrystals of HIV-1 RT with structurally different nonnucleoside inhibitors have been reported, showing that most ligands bind in a similar “butterfly-like” conformation to a hydrophobic pocket near the polymerase active site.

Our goal was to transfer the knowledge of binding requirements for NNRTIs, as deduced from crystal-

Chart 1. The PDB Code of the Selected Ligand/Enzyme Complexes, and the Names and the 2D-Structures of the Corresponding NNRTIs



lographic data, into a common three-dimensional chemical feature-based pharmacophore model that could be used to design new potentially active compounds.

Among all the available X-ray structures of wild-type HIV-1 RT in complex with a second generation NNRTI, we selected seven complexes based on the chemical uniqueness of the corresponding inhibitor and the resolution of the crystals.^{5–11}

Moreover, since most NNRTIs are known to be engaged in hydrogen bonding interactions with the backbone of the amino acids Lys101 and/or Lys103, we selected only those ligands that establish hydrogen bonds with these RT residues. Thus, the training set (TS) was composed of the following NNRTIs: efavirenz, MKC442 (emivirine), HBY097, MSC204, UC781, 739W94, and TMC120 (Chart 1).

The common features hypothesis generation approach (HipHop) implemented in the program Catalyst 9.0¹²

* To whom correspondence should be addressed. Phone: (++39) 090-6766464. Fax: (++39) 090-355613. E-mail: barreca@pharma.unime.it; a.rao@pharma.unime.it.

[‡] Università di Messina.

[‡] Istituto di Genetica Molecolare IGM-CNR.

[§] Rega Institute for Medical Research.

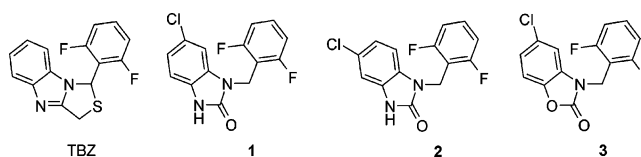
Table 1. Summary of the Common Feature Hypothesis Run

number ^a	composition ^b	ranking score ^c	direct hit mask ^d	partial hit mask ^e
Hypo 1	HHDA	56.5018	1111111	0000000
Hypo 2	HHDA	51.8973	1111111	0000000
Hypo 3	HHHA	51.1017	1111111	0000000
Hypo 4	HHHA	50.3632	1111111	0000000
Hypo 5	HHDA	48.9869	1111111	0000000
Hypo 6	HHHA	46.7207	1111111	0000000
Hypo 7	HHA	33.1821	1111111	0000000
Hypo 8	HHD	30.3244	1111111	0000000
Hypo 9	HDA	26.0421	1111111	0000000

^a Numbers for the hypothesis are consistent with the numeration as obtained by the hypothesis generation. ^b H: hydrophobic group; A: hydrogen bond acceptor. D: hydrogen bond donor. ^c The higher the ranking score, the less likely it is that the molecules in the TS fit the hypothesis by a chance correlation. Best hypotheses have highest ranks. ^d Direct hit mask: a TS molecule mapped every feature in the hypothesis. 1 means yes and 0 means no. ^e Partial hit mask: a TS molecule mapped all but one feature in the hypothesis. 1 means yes and 0 means no.

took into account the features of these seven compounds and found the 3D arrangement of functional groups common to all that interact with the RT enzyme, thus carrying out a “qualitative model”. We considered this the most appropriate approach because the “quantitative” hypothesis generation method is not suitable seeing that, owing to the different experimental protocols employed, the available biological data are not homogeneous.

Nine hypotheses, with the ranking scores ranging from 56.50 to 26.04, were thus obtained as described in the Supporting Information, and the results are presented in Table 1. As expected, our ligand-based hypothesis was in agreement with the structure-based information: in fact, the first (Hypo 1) and the second (Hypo 2) ranked pharmacophore models contained one hydrogen bond acceptor and one hydrogen bond donor group that bind with the target making key interactions (Table 1 and Figure 1). Moreover, this procedure provided further information about the precise disposition of the hydrophobic groups. In fact, even if Hypo 1 and 2 had the same chemical features (two hydrophobic

Chart 2. Structures of TBZ and Compounds 1–3

regions, one hydrogen bond acceptor and one hydrogen bond donor), one hydrophobic group, namely HY2 and HY3 in Figure 1, was differently located. In particular, in the selected NNRTIs, HY3 represents a portion, such as a chlorine atom or a methoxy group, which points into the hydrophobic pocket formed by the hydrocarbon chains of Val106, Phe227, Leu234, and Pro236. On the contrary, both aliphatic and aromatic moieties can occupy the chemical feature HY2, making hydrophobic contacts with the side chain of Leu100, Val106, Tyr318, Leu234, and Pro236.

Since both Hypo 1 and Hypo 2 represented plausible pharmacophore models for NNRTIs and considering that Hypo 3 showed all the three hydrophobic features (HY1–HY3), Hypo 1 and Hypo 2 were merged by using 0.8 Å tolerance, leading to a final model containing three lipophilic parts satisfying the steric and lipophilic requirements of the enzyme pocket.

Figure 1 shows the alignment of the 3D coordinates of the bound ligand efavirenz (the most active NNRTI clinically approved so far) onto the 3D merged five-feature hypothesis: the HBA and HBD are mapped by the carboxamide group, while the three hydrophobic sites HYs are mapped by the cyclopropyl group (HY1), the benzene-fused ring (HY2), and the chlorine atom (HY3) (see Supporting Information for mapping of the seven NNRTIs into the merged pharmacophore model).

Recently a ligand-based pharmacophore model of NNRTIs has been reported,¹³ which however presents two hydrophobic features in a different 3D arrangement.

Rational Drug Design. In previous papers we described a series of 1-aryl-1*H*,3*H*-thiazolo[3,4-*a*]benzimidazoles which proved to be highly active as HIV-1 NNRTIs. Extensive structure–activity relationship stud-

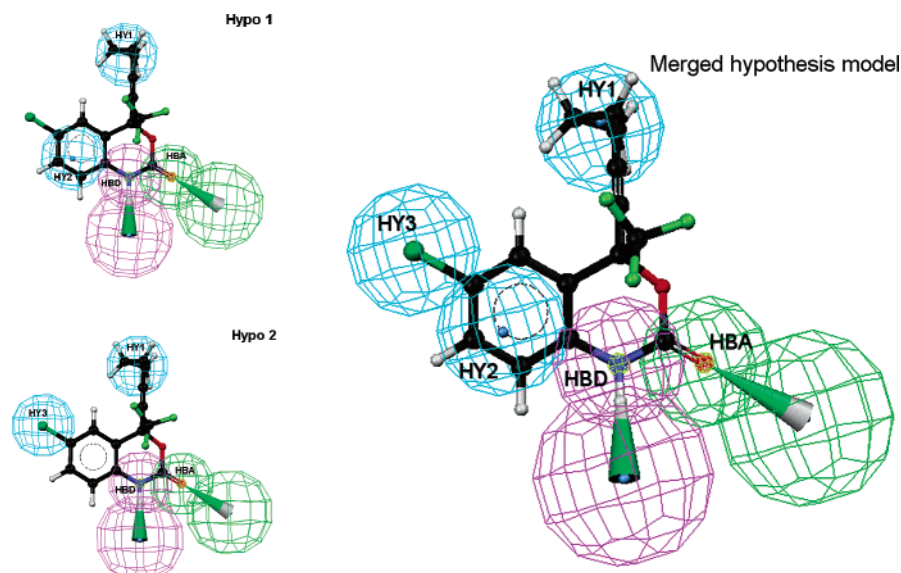


Figure 1. Efavirenz mapped into Hypo 1 (top left), Hypo 2 (bottom left), and merged hypothesis of nonnucleoside inhibitors of HIV-1 RT. The final pharmacophore model contains five features (HBD, hydrogen bond donor, purple; HBA, hydrogen bond acceptor, green; HY1–3, hydrophobic regions, cyan).

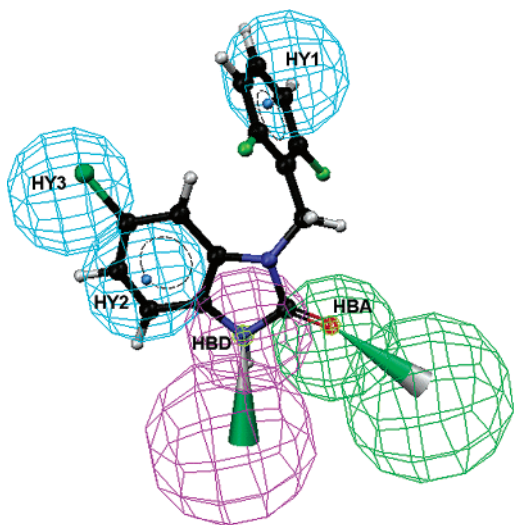


Figure 2. 3D-common features pharmacophore model of NNRTIs aligned to compound **1**.

ies led to the discovery of TBZ (Chart 2) as lead compound,⁴ whose binding mode into the lipophilic pocket of the enzyme was demonstrated to be similar to other NNRTIs. However, the fitting of TBZ into the obtained pharmacophore model lacked the features necessary to form hydrogen bond interaction with the Lys101 and/or Lys103 of the enzyme. On this basis, we reasoned that suitable chemical modifications of this molecule might lead to new classes of NNRTI candidates. The tricyclic system of TBZ was opened at the thiazole nucleus level, removing the sulfur atom, which in vivo is oxidized, giving less active or inactive metabolites. The conversion of the 1*H*-benzimidazole nucleus into the 1,3-dihydro-2*H*-benzimidazol-2-one system could generate a class of molecules that not only fit equally well into the allosteric site but also have the functional groups able to act as hydrogen bond acceptor and donor. Furthermore, a chlorine atom was introduced at position 6 of the benzimidazolone system, seeing that a *p*-chloroanilino moiety is a structural fragment present in many potent NNRTIs such as efavirenz. As shown in Figure 2, the designed compound **1** was able to fulfill the pharmacophore hypothesis. To verify whether the chlorine position could influence the inhibitory effects on

RT, we also planned the synthesis of 5-chloro derivative **2**. Finally, to prove the importance of the NH group as hydrogen bond donor, we designed the isostere benzoxazolone **3** which, lacking this functionality necessary to interact with the carbonyl backbone of residues Lys101, should have been less active than **1**. The structures of the designed derivatives **1–3** are reported in Chart 2.

Molecular Docking of Compounds 1–3. We sought to validate our hypothesis by performing automated docking studies of the designed compounds using Autodock 3.0.5.¹⁴ First of all, as in the docking calculations the ligands are flexible while the protein coordinates are fixed, test docking calculations using the seven selected ligands were carried out to validate the docking protocol and to confirm that the enzyme coordinates from the efavirenz/RT complex could be used to reproduce the binding mode of any NNRTI. The ligands were extracted from the corresponding RT complexes and then docked back into the allosteric pocket of the crystal structure 1FK9. The best Autodock-predicted conformation of all NNRTIs agreed well with the experimental binding mode of these ligands, with root-mean square deviations (RMSD) < 1 Å (see Supporting Information).

Later, docking of compounds **1–3** into the RT allosteric site generated a number of possible binding conformations that correlated with energies. The cluster analysis revealed a predominant ligand orientation within the binding pocket (65, 40, and 21 conformations in the first ranked cluster for **1**, **2**, and **3**, respectively), and the most energetically favorable conformation for each ligand was chosen for further analysis.

The best docked conformation of compound **1** is shown in Figure 3, together with the experimental position of efavirenz and the 3D common-feature pharmacophore model. Compound **1** interacted in a fashion similar to known NNRTIs with RT residues of the allosteric pocket. In fact, in agreement with the mapping of the designed molecule into the merged hypothesis, the carboxamide group of the molecule interacted with the main-chain of Lys101 by hydrogen bond interactions, while the hydrophobic features HY1–HY3 are occupied by the *p*-chloroanilino and 2,6-difluorophenyl moieties.

The superimposition of the docked compound **2** and the pharmacophore model demonstrated a different

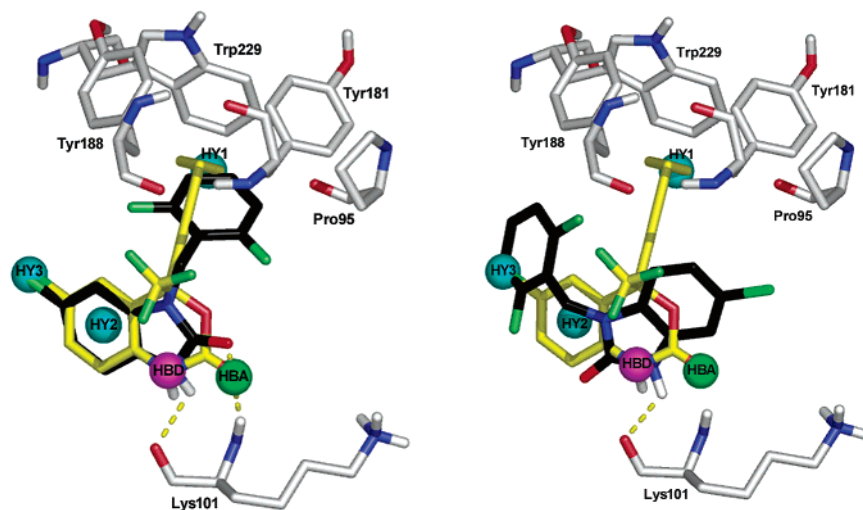
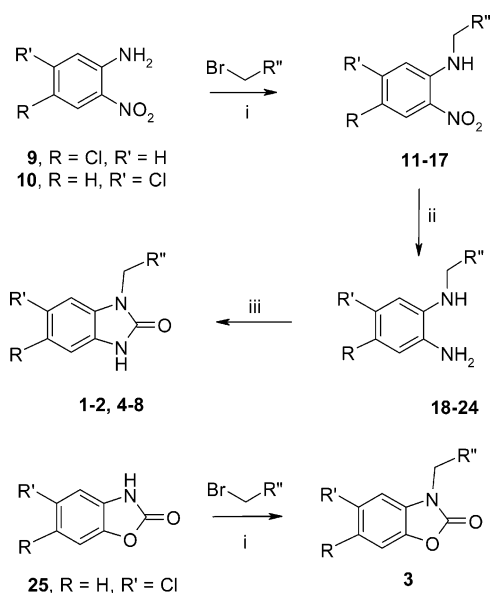


Figure 3. AutoDock-predicted binding mode of **1** (left) and **2** (right) compared to the crystallized position of Efavirenz (yellow). The colored spheres represented the 3D pharmacophore model developed by HipHop/Catalyst.

Scheme 1^a

Compd	R	R'	R''
1, 3, 11, 18	H	Cl	2,6-difluorophenyl
2, 12, 19	Cl	H	2,6-difluorophenyl
4, 13, 20	H	Cl	2,6-dichlorophenyl
5, 14, 21	H	Cl	4- <i>i</i> -propylphenyl
6, 15, 22	H	Cl	α -naphthyl
7, 16, 23	H	Cl	β -naphthyl
8, 17, 24	H	Cl	cyclohexyl

^a Reagents: (i) DMF, K₂CO₃, Δ , 2 h; (ii) Zn/HCl, EtOH, 80 °C, 1 h; (iii) 20% toluene solution of COCl₂, 2 N HCl, Δ , 4 h.

Table 2. Anti-RT and Anti-HIV-1 Activities, Cytotoxicity, and Selectivity Index in MT-4 Cells

compd	IC ₅₀ (μ M) ^a	EC ₅₀ (μ M) ^b	CC ₅₀ (μ M) ^c	SI ^d
1	2.86 \pm 0.1	0.24 \pm 0.05	>424	>1766
2	60 \pm 4	29.6 \pm 2.1	>424	>14
3	20 \pm 1.5	3.72 \pm 0.47	>382.2	>91
4	7.50 \pm 0.5	3.79 \pm 1.68	315 \pm 25.9	83
5	16.2 \pm 0.8	2.83 \pm 1.26	>415	>147
6	12.7 \pm 0.5	0.87 \pm 0.16	50.0 \pm 2.43	57
7	5.20 \pm 0.5	6.35 \pm 0.92	>405	>64
8	50 \pm 8	NA	9.50 \pm 1.72	
TBZ	24.57 \pm 2	1.10 \pm 0.32	50.0 \pm 3.2	45

^a Concentration required to inhibit by 50% the *in vitro* RNA-dependent DNA polymerase activity of recombinant RT. ^b Effective concentration required to reduce HIV-1-induced cytopathic effect by 50% in MT-4 cells. ^c Cytotoxic concentration required to reduce MT-4 cell viability by 50%. ^d Selectivity index: ratio CC₅₀/EC₅₀. NA = not active.

binding mode compared to **1** and less efficient hydrophobic/hydrogen-bond interactions with the surrounding residues in the allosteric site (Figure 3). In particular, it was surprising to note that this molecule did not map the feature HY1, lacking any hydrophobic contact with the region of the enzyme formed by Pro95, Leu100, Tyr181, Tyr188, Trp229, and Leu234. Finally, even if compound **3** docked in a position and orientation similar

to **1**, as expected there was only one hydrogen bond interaction between the carbonyl group of the ligand and the backbone of the Lys101 residue.

On the basis of these molecular modeling results, we designed other 1*H*,3*H*-thiazolo[3,4-*a*]benzimidazole derivatives (i.e. **4–8**) in which the 6-chlorine substitution was maintained, whereas the 2,6-difluorophenyl moiety was suitably modified or replaced to enhance the steric hindrance or the lipophilicity.

Chemistry. The synthesis of compounds **1–8** was realized according to the reaction sequence reported in Scheme 1. The 2-nitroaniline (**9** or **10**) was N-alkylated by treatment with the appropriate alkyl bromide in the presence of potassium carbonate to give intermediates **11–17** which were reduced with Zn dust in acidic medium. The cyclization of the amino derivatives **18–24** with phosgene afforded target compounds **1, 2, 4–8**. Compound **3** was obtained by N-alkylation of the commercially available 5-chloro-3*H*-benzoxazol-2-one (**25**).

Anti-HIV Activity Assays. Compounds **1–8** were tested in RT inhibition assays and proved to be active as inhibitors of HIV-1 RT (Table 2). The enzymatic data highlighted that derivative **1** turned out to be more active than TBZ: targeting the enzyme for hydrogen bond donor/acceptor interactions was thus a valid strategy to increase RT inhibitory activity of the starting compound. As shown by the inhibition profile of compounds **1** and **2**, the position of the halogen substituent on the benzene ring influenced the affinity. In fact, the presence of a chlorine substituent at C-5 led to a decrease of potency, confirming that, as prompted by the molecular docking experiments, the chlorine atom at position 6 may lead to a binding conformation resulting in improved hydrophobic contacts with the surrounding residues in the binding site.

Compound **3** was 1 order of magnitude less active than **1**; this result was also consistent with our hypothesis and clearly demonstrated the importance of the hydrogen bond interaction of the NH group with the carbonyl backbone of Lys101.

Considering the effect of the substituent at N-1, the replacement of the 2,6-difluorophenyl moiety with other aromatic or aliphatic groups negatively influences the RT inhibitory activity. However, 2,6-dichlorophenyl (**4**), 4-*i*-propylphenyl (**5**), and naphthyl (**6** and **7**) derivatives showed a good level of inhibitory activity whereas cyclohexyl-substituted compound (**8**) is totally inactive. This finding underlines the importance of the aromatic moiety for this class of inhibitors.

Compounds **1–8** were also evaluated for inhibition of the cytopathic effects of HIV-1 (III_B) in MT-4 cells. Compound-induced cytotoxicity was also measured in MT-4 cells in parallel with the antiviral activity (Table 2). The results of this test provided the confirmation that our rational design project worked since compound **1** was more potent than TBZ in preventing the cyto-

Table 3. Anti-HIV-1 Activity of **1** and TBZ against Mutant HIV-1 Strains in CEM Cells

compd	EC ₅₀ (μ M) ^a					
	HIV-1 _{III_B}	L100I	K103N	E138K	Y181C	Y188H
1	0.88 \pm 0.51	2.0 \pm 1.4	>20	2.9 \pm 2.2	>20	>20
TBZ	1.39 \pm 0.56	3.12 \pm 0.94	15.6 \pm 3.2	1.73 \pm 1.02	13.8 \pm 4.2	4.16 \pm 1.12

^a Effective concentration to protect CEM cells against the cytopathogenicity of HIV-induced by 50%.

pathic effect of HIV-1 and was minimally toxic to MT-4 cells, resulting in a remarkably high selectivity index. Compound **1** was also tested in CEM cell cultures against an extensive panel of mutant virus strains containing in their RT a single mutation that is characteristic of the HIV-NNRTI resistance profile. The compound generally kept activity against L100I and E138K RT HIV-1, but lost antiviral activity against K103N, Y181C, and Y188H RT HIV-1 strains (Table 3).

Conclusions. A combined ligand- and structure-based molecular modeling approach led to the design of potential NNRTIs structurally related to our previously reported 1*H*,3*H*-thiazolo[3,4-*a*]benzimidazoles. A simple synthetic route of novel 1,3-dihydro-2*H*-benzimidazol-2-ones has been developed. Biological results showed compound **1** as a starting point for lead optimization strategy, which is already ongoing.

Experimental Section

Chemistry: **5-Chloro-1-(2,6-difluorobenzyl)-2-nitroaniline (11).** To a stirred solution of 5-chloro-2-nitroaniline (**10**) (346 mg, 2 mmol) in DMF (10 mL) were added 2,6-difluorobenzyl bromide (621 mg, 3 mmol) and anhydrous potassium carbonate (1.382 mg, 10 mmol). The reaction mixture was refluxed for 2 h, cooled, filtered and, after addition of water (60 mL), extracted with chloroform (2 × 50 mL). After removal of the solvent under reduced pressure, the residue was powdered by treatment with diethyl ether and recrystallized from ethanol. **4-Chloro-1-(2,6-difluorobenzyl)-2-nitroaniline (12).** With a similar procedure, **12** was prepared from 4-chloro-2-nitroaniline (**9**) (346 mg, 2 mmol) and 2,6-difluorobenzyl bromide (621 mg, 3 mmol). With a similar procedure and starting from **10**, we have prepared: **5-chloro-1-(2,6-dichlorobenzyl)-2-nitroaniline (13)** with 2,6-dichlorobenzyl bromide (720 mg, 3 mmol); **5-chloro-1-(4-isopropylbenzyl)-2-nitroaniline (14)** with 4-*i*-propylbenzyl bromide (640 mg, 3 mmol); **5-chloro-1-(1-naphthyl)methyl-2-nitroaniline (15)** with (1-naphthyl)methyl bromide (663 mg, 3 mmol); **5-chloro-1-(2-naphthyl)methyl-2-nitroaniline (16)** with (2-naphthyl)methyl bromide (663 mg, 3 mmol); **5-chloro-1-(cyclohexylmethyl)-2-nitroaniline (17)** with cyclohexylmethyl bromide (531 mg, 3 mmol).

2-Amino-5-chloro-1-(2,6-difluorobenzyl)aniline (18). The mixture of **11** (179 mg, 0.6 mmol) in 3 mL of HCl and 4 mL of EtOH was stirred vigorously, then zinc dust (1.32 g, 20 mmol) was added in several portions at room temperature. After this addition was completed, the reaction mixture was heated on a water bath for 1 h, cooled, made alkaline with 2 N NaOH, and then extracted with ethyl acetate. The extracted was washed with water, dried over Na₂SO₄, and evaporated. The residue was crystallized from ethanol. With a similar procedure, we have prepared: **2-amino-4-chloro-1-(2,6-difluorobenzyl)-aniline (19)** from **12** (149 mg, 0.5 mmol); **2-amino-5-chloro-1-(2,6-dichlorobenzyl)-aniline (20)** from **13** (166 mg, 0.5 mmol); **2-amino-5-chloro-1-(4-isopropylbenzyl)-aniline (21)** from **14** (145 mg, 0.5 mmol); **2-amino-5-chloro-1-(1-naphthyl)methyl-aniline (22)** from **15** (155 mg, 0.5 mmol); **2-amino-5-chloro-1-(2-naphthyl)methyl-aniline (23)** from **16** (155 mg, 0.5 mmol); **2-amino-5-chloro-1-(cyclohexylmethyl)-aniline (24)** from **17** (135 mg, 0.5 mmol).

6-Chloro-1-(2,6-difluorobenzyl)-1,3-dihydro-2*H*-benzimidazol-2-one (1). To a solution of **18** (67 mg, 0.25 mmol) in 2 N HCl (4 mL) was added an excess of a 20% toluene solution of phosgene (1 mL), and the resulting mixture was heated for 4 h. After cooling, the reaction mixture was neutralized with 2 N NaOH, extracted with ethyl acetate, washed with water, and evaporated under reduced pressure. The residue was crystallized from ethyl acetate. With a similar procedure, we have prepared: **5-Chloro-1-(2,6-difluorobenzyl)-1,3-dihydro-2*H*-benzimidazol-2-one (2)** from **19** (67 mg, 0.25 mmol); **6-Chloro-1-(2,6-dichlorobenzyl)-1,3-dihydro-2*H*-benzimidazol-2-one (4)** from **20** (75 mg, 0.25 mmol); **6-Chloro-1-(4-isopropylbenzyl)-1,3-dihydro-2*H*-benzimidazol-2-one (5)** from **21** (69 mg, 0.25 mmol); **6-Chloro-1-(1-naphthyl)methyl-1,3-dihydro-2*H*-benzimidazol-2-one (6)** from **22** (70 mg, 0.25 mmol); **6-Chloro-1-(2-naphthyl)methyl-1,3-dihydro-2*H*-benzimidazol-2-one (7)** from **23** (70 mg, 0.25 mmol); **6-Chloro-1-(cyclohexylmethyl)-1,3-dihydro-2*H*-benzimidazol-2-one (8)** from **24** (60 mg, 0.25 mmol).

5-Chloro-3-(2,6-difluorobenzyl)-3*H*-benzoxazol-2-one (3). Compound **3** was synthesized with a procedure similar to that reported for **11**, starting from chlorzoxazone (**25**) (170 mg, 1 mmol) and 2,6-difluorobenzyl bromide (310 mg, 1.5 mmol).

Acknowledgment. Financial support for this research by Fondo Ateneo di Ricerca (2002, Messina, Italy), MIUR (COFIN2002, Roma, Italy), and the European Commission (QLK2-CT-2000-00 291) is gratefully acknowledged.

Supporting Information Available: Additional experimental data are available free of charge via Internet at <http://pubs.acs.org>.

References

- De Clercq, E. Antiviral drugs in current clinical use. *J. Clin. Virol.* **2004**, *30*, 115–133.
- Balzarini, J. Current status of the nonnucleoside reverse transcriptase inhibitors of human immunodeficiency virus type 1. *Curr. Top Med. Chem.* **2004**, *4*, 921–944.
- Barreca, M. L.; Balzarini, J.; Chimirri, A.; De Clercq, E.; De Luca, L.; et al. Design, synthesis, structure–activity relationships, and molecular modeling studies of 2,3-diaryl-1,3-thiazolidin-4-ones as potent anti-HIV agents. *J. Med. Chem.* **2002**, *45*, 5410–5413.
- Chimirri, A.; Grasso, S.; Molica, C.; Monforte, A. M.; Monforte, P.; et al. Structural features and anti-human immunodeficiency virus (HIV) activity of the isomers of 1-(2',6'-difluorophenyl)-1*H*,3*H*-thiazolo[3,4-*a*]benzimidazole, a potent nonnucleoside HIV-1 reverse transcriptase inhibitor. *Antiviral Chem. Chemother.* **1997**, *8*, 363–370.
- Ren, J.; Milton, J.; Weaver, K. L.; Short, S. A.; Stuart, D. I.; et al. Structural basis for the resilience of efavirenz (DMP-266) to drug resistance mutations in HIV-1 reverse transcriptase. *Structure Fold Des.* **2000**, *8*, 1089–1094.
- Hopkins, A. L.; Ren, J.; Esnouf, R. M.; Willcox, B. E.; Jones, E. Y.; et al. Complexes of HIV-1 reverse transcriptase with inhibitors of the HEPT series reveal conformational changes relevant to the design of potent nonnucleoside inhibitors. *J. Med. Chem.* **1996**, *39*, 1589–1600.
- Hsiou, Y.; Das, K.; Ding, J.; Clark, A. D., Jr.; Kleim, J. P.; et al. Structures of Tyr188Leu mutant and wild-type HIV-1 reverse transcriptase complexed with the nonnucleoside inhibitor HBY 097: inhibitor flexibility is a useful design feature for reducing drug resistance. *J. Mol. Biol.* **1998**, *284*, 313–323.
- Hogberg, M.; Sahlberg, C.; Engelhardt, P.; Noreen, R.; Kangas-metsa, J.; et al. Urea-PETT compounds as a new class of HIV-1 reverse transcriptase inhibitors. 3. Synthesis and further structure–activity relationship studies of PETT analogues. *J. Med. Chem.* **2000**, *43*, 304.
- Ren, J.; Esnouf, R. M.; Hopkins, A. L.; Warren, J.; Balzarini, J.; et al. Crystal structures of HIV-1 reverse transcriptase in complex with carboxanilide derivatives. *Biochemistry* **1998**, *37*, 14394–14403.
- Chan, J. H.; Hong, J. S.; Hunter, R. N., 3rd; Orr, G. F.; Cowan, J. R.; et al. 2-Amino-6-arylsulfonylbenzimidazoles as nonnucleoside reverse transcriptase inhibitors of HIV-1. *J. Med. Chem.* **2001**, *44*, 1866–1882.
- Das, K.; Clark, A. D., Jr.; Lewi, P. J.; Heeres, J.; De Jonge, M. R.; et al. Roles of conformational and positional adaptability in structure-based design of TMC125–R165335 (etravirine) and related nonnucleoside reverse transcriptase inhibitors that are highly potent and effective against wild-type and drug-resistant HIV-1 variants. *J. Med. Chem.* **2004**, *47*, 2550–2560.
- Catalyst 4.9, Accelrys Inc., San Diego, <http://www.accelrys.com>.
- Patel, Y.; Gillet, V. J.; Bravi, G.; Leach, A. R. A comparison of the pharmacophore identification programs: Catalyst, DISCO and GASP. *J. Comput.-Aided Mol. Des.* **2002**, *16*, 653–681.
- Morris, G. M.; Goodsell, D. S.; Halliday, R. S.; Huey, R.; Hart, W. E.; et al. Automated Docking Using a Lamarckian Genetic Algorithm and Empirical Binding Free Energy Function. *J. Comput. Chem.* **1998**, *19*, 1639–1662.

JM049279A